Gold cluster formation on C_{60} surfaces observed with scanning tunneling microscopy: Au-cluster beads and self-organized structures

Hui Liu, Petra Reinke *

University of Virginia, Department of Materials Science and Engineering, 395 McCormick Road, Charlottesville, VA 22904, USA

Abstract

The growth mechanism of Au-clusters on fullerene layers has been investigated by scanning tunneling microscopy in ultrahigh vacuum at room temperature. The fullerene layers, which serve as substrates, are formed on a graphite surface and exhibit the typical combination of round and fractal shapes, and small sections of the original graphite substrate are exposed. The immobile Au-clusters are concentrated on the C_{60} terminated surface section, and the original fullerene island structures are preserved. A preferential nucleation of Au-clusters is observed at the C_{60}–graphite edges while the C_{60}–C_{60} edges remains undecorated. These Au-clusters are placed directly on the edge and shared by the graphite and fullerene layer. They form bead-like structures, which densely populate this edge, while the first layer C_{60} islands are clearly depleted of Au-clusters. A roughness analysis of the fullerene surface indicates the presence of Au atoms (or very small clusters), which are embedded in the fullerene surface, and likely situated in the troughs in between the large molecules. These Au atoms are highly mobile and cannot be individually resolved at room temperature. The analysis of the spatial and size distributions of Au-clusters provides the basis for the development of a qualitative model, which describes the relevant surface processes in the Au–fullerene system. The simultaneous deposition of Au and fullerene on graphite leads to the formation of highly organized structures, in which Au-clusters are embedded in a ring of fullerene molecules with a constant width of about 4 nm. The mechanism for the formation of these structures is highly speculative at present and further experiments will be pursued in the near future. A comprehensive analysis of the Au–C_{60} system is presented, which contributes to the advancement in our understanding of the metal–fullerene interaction and furthers the development of composite materials of interest in the synthesis of solar cells and metal contacts to organic materials.
© 2007 Elsevier B.V. All rights reserved.

1. Introduction

Fullerenes, and in particular C_{60}, have attracted considerable attention since their discovery in 1985 and are studied intensely due to their unique properties [1–5]. The modification of fullerene solids through exohedral or endohedral doping further broadens the spectrum of properties, and allows modifying and adapting the electronic structure of this molecular solid. Fullerenes have been shown to per-

form as superconductors [1], in optical devices [3] and microsensors [6], and are an integral part of novel organic solar cells [7], where they act as electron acceptor. The current interest in fullerenes is driven by their incorporation in nanotechnology applications, and the fundamental questions related to the electronic structure of molecular solids.

In order to utilize fullerene-based materials and incorporate them in nanoscale electronics, information about the metal–C_{60} interaction is indispensable. The interaction of C_{60} with gold and other metal and semiconductor surfaces has been studied extensively in the past decade [6,8–15], usually by the deposition of fullerenes on a reconstructed

---

* Corresponding author. Tel.: +1 434 9247203.
E-mail address: pr6e@cms.mail.virginia.edu (P. Reinke).

well-defined surface. On the other hand, the interaction of metal or semiconductor atoms with the fullerene surface has garnered much less attention, despite the importance of this process for the formation of metal contacts [2,16]. With the present study we explore the Au–C_{60} system in an effort to understand how metal clusters and C_{60} interact physically and electronically. We concentrate here on the structural aspects, and early stages of Au-overlayer growth, which was investigated with scanning tunneling spectroscopy (STM). This study is a continuation of our previous work on the electronic interaction and bonding of Si and Au with the C_{60} surface [17,18]. In our previous work, we used photoelectron spectroscopy to analyze the formation of Au-clusters on the C_{60} surface, and observed the cluster formation as a function of Au-coverage. The analysis of the d-band splitting (initial state) and the Au4f core level shift due to delayed photohole relaxation (final state effect) is used to characterize the cluster growth process. The chemisorption interaction between fullerenes and Au-clusters, and the electronic characteristics of the Au–fullerene interface were deduced from the core level and valence band spectra. However, the geometrical arrangement of the Au-clusters with respect to the fullerene lattice and the details of the cluster size and shape distribution remained an open question, which could only be approached with an imaging method such as STM.

In the present study, we investigate the interaction of Au with a C_{60} surface by observing the accumulation of Au and Au-cluster formation with scanning tunneling microscopy. We also explore the regime of high mobility for both reactants by co-deposition of Au and C_{60} molecules, a process which leads to the formation of characteristic, self-organized Au cluster–C_{60} structures. A prerequisite for this set of experiments is the deposition of the fullerene layer on a weakly interacting substrate such as graphite, which also eliminates charge transfer between substrate and fullerene layer. These C_{60} layers provide various local environments, such as edges, kinks and extended C_{60} regions, for the growth of Au-clusters [19]. The C_{60} surface itself is highly corrugated and the troughs and grooves between the molecules provide high-coordination bonding sites. We will first describe the topography of Au-deposition on C_{60} layers, and analyze the cluster formation, size distribution and shapes. Subsequently, we describe the atomic level topography and develop a model for the growth process. The last section is devoted to a discussion of the co-deposition process and the feasibility of self-organization within metal–C_{60} structures.

2. Experimental

The experiments were performed in an Omicron Variable Temperature ultrahigh vacuum scanning probe microscope (Omicron VT UHV-SPM) system that consists of a preparation chamber and an analysis chamber containing the microscope. The sample can be transferred between the chambers without breaking the vacuum and the back-

ground pressure was 2×10^{-10} mbar. Atomically flat HOPG surfaces were obtained by the removal of the top layer with scotch-tape in air, and subsequent annealing at 300 °C for at least 10 h in the UHV chamber prior to deposition. The C_{60} beam was created by thermal sublimation of commercially available high-purity C_{60} powder (Mer-Corp) from a BN-crucible.

Subsequently, Au was deposited on the HOPG/C_{60} layer at a rate of approximately 0.2–0.4 nm/s. The Au-source consisted of a cooling shroud, which contained a resistively heated molybdenum wire intertwined with a Au-wire. The deposition experiments of Au were carried out in a cumulative manner and STM images were recorded after each deposition event. Co-deposition of Au and C_{60} was performed with roughly equal deposition rates for both components of around 0.2–0.4 nm/s. Deposition rates were calibrated from the STM images.

All STM images were acquired in the constant current mode at room temperature and are displayed such that the scan lines are horizontal and scanning proceeds from the bottom to the top. Chemically etched tungsten wires were used as STM tips. The STM images were, unless otherwise stated, recorded with a sample bias voltage of 1.2 V and the tunneling current of 0.1 nA. The image of C_{60} with Au on top remains undisturbed at a bias voltage of as low as 0.6 V provided that the tip condition was excellent. With a bias voltage of 0.1 V, the tip removes most of C_{60} molecules from the scanned area, while the Au clusters remain at their original positions.

3. Results

Fig. 1 illustrates the growth progression of Au-clusters deposited on a multilayer HOPG–C_{60} film. The first image (Fig. 1a) shows the characteristic mixed growth mode, which has been observed in the growth of C_{60} layers on HOPG. The first layer of C_{60} in contact with the graphite surface grows in elliptically shaped, relatively large islands, and all subsequent layers form small fractal-dendritic islands, which nucleate in the center of the first layer fullerene islands. The different mobilities of C_{60} on C_{60} surfaces and on graphite lead to the formation of these distinct island structures and a detailed description of the C_{60} layer growth on graphite is given in Ref. [19]. The image in Fig. 1a is intersected by a straight graphite step edge, which functions as a nucleation center for the first layer islands and acts at the same time as a diffusion barrier leading to nucleation of new islands on both sides of the step. These images, recorded prior to the deposition of Au, also show a large number of streak-like features on the uncovered graphite surface, which are attributed to highly mobile molecules moved through the interaction with the STM tip [8,20,21]. After the deposition of Au, the characteristic length of the streaks is increased, their frequency is reduced and the sawtooth shape of the trace disappears. The short sawtooth shaped streaks, which are characteristic for tip-induced molecule movement, are rarely observed after the
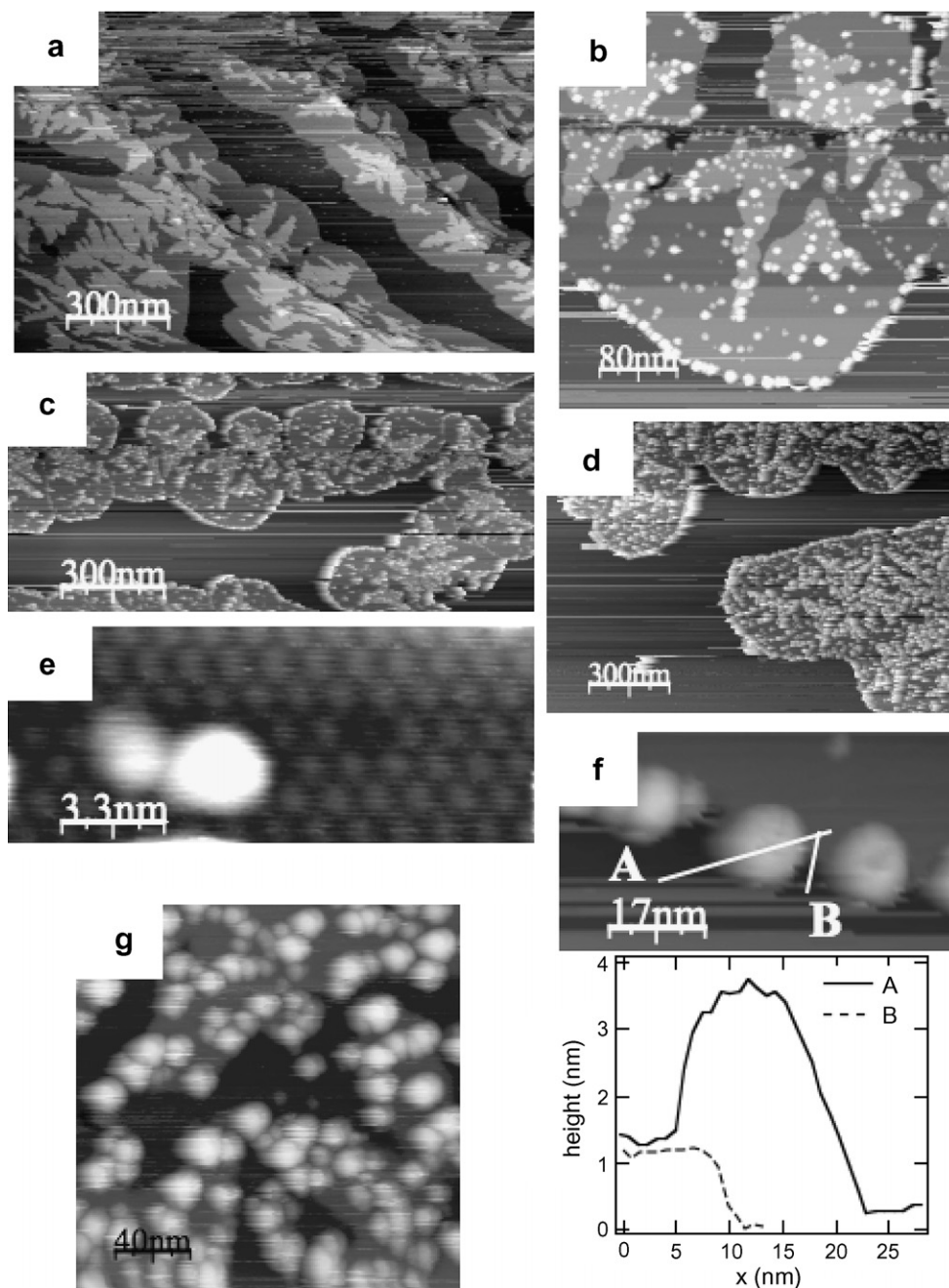
Fig. 1. These STM images show the characteristic features, which develop during the deposition of Au on C_{60} thin films (on HOPG as substrate). (a) C_{60} deposited on bare HOPG, no Au has been deposited. The lines intersecting the fullerene islands are steps which are present in the original graphite surface. The large round islands (first layer) and the fractal shaped islands (second and subsequent layers) are composed of C_{60}. A linescan confirmed the layer thickness. (b) and (c) are obtained after the deposition of Au on the substrate (HOPG–C_{60}) shown in (a), the cumulative deposition time is 9 s. (d) The cumulative deposition time of Au is 15 s; the round, small islands correspond to Au-clusters. (e) High-resolution image of Au clusters on C_{60} with a point defect in the fullerene lattice (center of image) and two Au-clusters. (f) Au-clusters are positioned right on the edge, half on the HOPG and half on the C_{60} layer; the two line scans, which are indicated in the image for path A and B confirm the location of the Au-clusters with respect to the edge. (g) This image was taken on a first layer fullerene island (high Au-coverage, see image (d) for an overview). The dark background is the surface of the first layer fullerene, the light gray sections are the surface of the second layer fullerenes. The Au-clusters reside preferentially on the second layer islands.

Au-deposition. Au-clusters with diameters exceeding about 1.5 nm are immobile on the fullerene surface and therefore easily imaged, which is in contrast to the high mobility of Au-clusters on graphite surfaces described by Hoevel et al. [22]. To prevent the movement of the Au-clusters on graphite, extended defect structures had to be created

which served to anchor larger Au-clusters ($d > 10$ nm on average), and enabled Hoevel et al. to observe Au-cluster geometry and electronic structure in considerable detail.

The images in Fig. 1b–d show the accumulation of Au on the surface: the low-coverage, image Fig. 1b and c corresponding to 9 s deposition time, the high-coverage in

image Fig. 1d and g are obtained after a cumulative depo-sition time of 15 s. The Au-clusters are concentrated on the C_{60} terminated surface section and remain stationary dur-ing imaging. It is remarkable that the basic features of the original C_{60} island structures is preserved: the density of Au-clusters on the second C_{60} layer with the fractal structure is larger than on the first layer C_{60} surface, and the outline of the second layer island can therefore be clearly discerned. The edges of first C_{60} layer are decorated by Au-clusters, and the Au-cluster density on the second layer fractal-dendritically shaped C_{60} islands exceeds the first layer density by about a factor of eight (Fig. 1b). An increase in the Au-coverage leads to an increase in the area density and cluster size. It is noted that many clusters are positioned in close proximity to each other at larger Au-coverage, and although they still retain a clearly discernible boundary their spherical shape is often distorted. Some of the larger clusters show a flat top, which might be attribut-able to the onset of faceting as described by Hoevel et al. [22]. The analysis of cluster dimensions is described in more detail in the next paragraph.

Fig. 1e is a high-resolution image, which shows the loca-tion of a few small Au-clusters on the surface and illus-trates that no preferential positioning of the clusters with respect to the C_{60} lattice is present. High-resolution images, where individual fullerene molecules are resolved, are rou-tinely achieved for all deposition conditions discussed here. These images are used to measure the surface roughness of the fullerene layers with and without Au-surface clusters as described in the next paragraph. The C_{60} lattice parameters are identical to pure C_{60} layers and image Fig. 1e includes a rarely observed point defect in the C_{60} lattice. In Fig. 1f, the HOPG–C_{60} edge is shown, and the Au-clusters are positioned right on the edge, half on the HOPG and half on the C_{60} layer. The density of edge-clusters increases with the Au-coverage and at high-coverage nearly continuous Au-cluster beads are formed and define the boundary between C_{60} and graphite. At lower Au-coverage those regions of the edge, which surround smaller areas of the graphite (see Fig. 1b), exhibit a smaller concentration of edge clusters. The edge between the first and second C_{60} layer is not decorated.

The cluster size distributions for the low and high Au-coverage are shown in Fig. 2. The size distribution on the first and second layer C_{60} islands, are equivalent within the error of the analysis but the cluster density differs con-siderably. The average cluster sizes are 7.7 ± 1.5 nm for the low-coverage and 9.5 ± 1.1 nm for the high-coverage, and the largest observed cluster size is 14 nm. However, the average size of clusters trapped on the C_{60}–graphite edge is 10.8 ± 1.7 nm, thus exceeding the average cluster size on the terraces. For the high-coverage, the size of the edge clusters could not be determined due to their close proxim-ity, which renders the analysis unreliable. The cluster sizes were obtained by using the full width at half maximum (FWHM size) of the linescan across the Au-cluster. The cluster diameter for the edge clusters was determined from
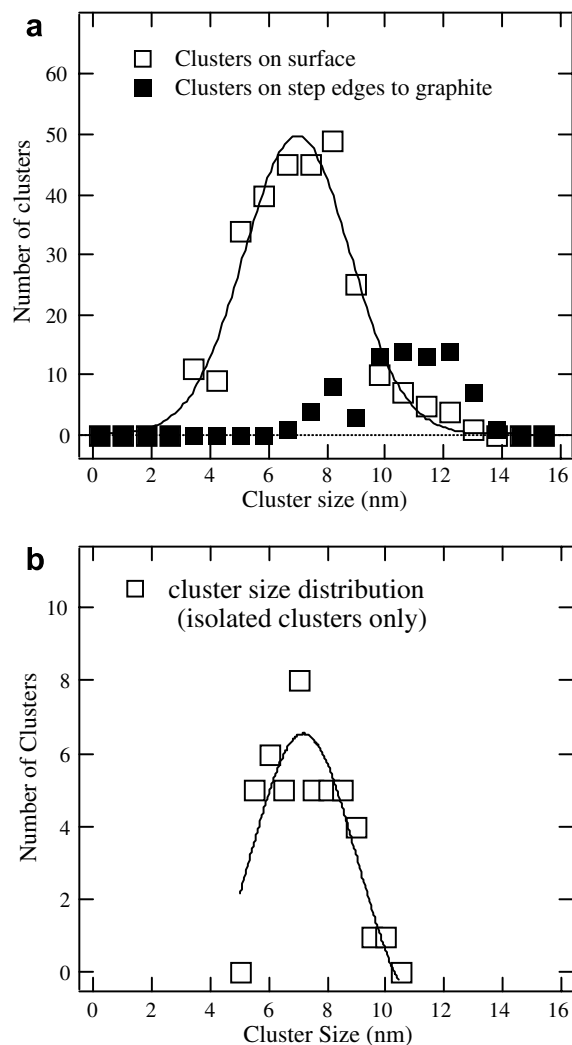

Fig. 2. Lateral size distributions of Au-clusters on C_{60} films, (a) shows the distributions for low-coverage of Au (compare Fig. 1b) and (b) includes the data for the high-coverage of Au obtained (Fig. 1c and d). The broken line serves as guidance for the eye.

the line profile across the cluster by marking the half height separately for each edge, and measuring the horizontal dis-tance between both points (parallel to axis). We chose this method to be able to compare our results with those of an analysis of the influence of tip–cluster interaction, which was introduced by Klyachko and Chen [23]. The number of clusters included in the size distribution is relatively small for the high-coverage sample since we did not include any clusters, which presented a deviation of the spherical shape due to close proximity of adjacent clusters or were strongly distorted by imaging artifacts. This necessary selection yields a representative sample for clusters exceed-ing 6 nm in diameter, but smaller clusters are usually sur-rounded by larger size ones, and their height and diameter cannot be measured reliably and was omitted. The number of clusters analyzed for the high Au-coverage and on the fullerene-edge is relatively small, and we there-fore refrain from a detailed analysis of the shape of the distributions.

The cluster size analysis with STM is always challenging since the image is a convolution of the tip and the true cluster shape. The steep sidewalls of the clusters interact with the tip side and the lateral extension of metal clusters is therefore overestimated, while the cluster height is measured correctly. Klyachko and Chen [23] recently described the effect of the tip convolution and its influence on the measured cluster size distribution in a quantitative model, which was tested in the analysis of isolated C_{60} molecules. We implemented their algorithm, and applied it to the Au cluster–C_{60} system. It is used to estimate how the cluster size distributions shown in Fig. 2 are modified due to tip–cluster interaction. In our model, the basic geometry from Klyatschko's model was used and an ideal Au-cluster of spherical shape is placed on the C_{60} surface. We used 0.2 nm as radius of the (atomically sharp) STM-tip apex and 0.65 nm as distance between tip apex and the center of C_{60} molecules. Another critical parameter is the distance between the tip and Au-cluster: a tunneling distance of 1.5 nm between the Au-cluster and the tip is used in our calculation, an estimate based on the work reported by Hasegawa et al. [24]. The results show that the cluster size can be overestimated by up to 3 nm when the real cluster size is 1 nm or less. For a real cluster size of 5 nm, the measured size is still 1.5 nm larger and the cluster will appear as 6.5 nm clusters in the distribution. A cluster with a diameter of nearly 6 nm, will also appear as a 6.5 nm cluster in the STM image and the width of the size distribution for smaller clusters is therefore reduced. The size distribution is less distorted for larger cluster sizes above 6.5 nm. The measured distributions shown in Fig. 2 therefore represent the larger cluster size quite well, but are inaccurate on the side of smaller clusters. The integral (total number of clusters) with a size of less than 6.5 nm is presented correctly. The cut-off of the distribution at 3 nm can be caused by the overestimation of cluster size of very small clusters inherent to the imaging method.

The imaging of small clusters, which are positioned on an insulating substrate, can be influenced by the occurrence of a Coulomb blockade [27–29], where the removal (or addition) of an electron leads to an increase in the electrostatic energy of the system by $e^2/2C$, where C is the capacitance of the assembly (cluster–tip-surface). For an electrically insulated cluster the discrete values of the charging energy associated with the transfer of a single charge are reflected in the appearance of steps in $I–V$ curves measured at the cluster site. The current is suppressed within the Coulomb gap and the tunneling current is reduced at low gap voltages leading to an apparent reduced height of the cluster. This effect has been reported for Au-clusters, which were immobilized on self-assembled monolayers made of alkyl-thiols where the Coulomb blockade can be observed even at room temperature.

In our samples, the $I–V$ curves were measured for several Au-clusters of various sizes and the typical signature for the Coulomb blockade could not be observed. The absence of a Coulomb blockade can be due to a relatively large cluster size, the differences in resistivity and capacitance of a fullerene layer compared to the alkyl chains, and the fact that the thermal energy exceeds at room temperature the charging energy for this particular system. All measurements were performed with a gap voltage of 1.2 V, which exceeds the magnitude of the expected Coulomb blockade gap for the given cluster size, and its influence on our present measurements is therefore estimated to be small. However, we concede that in order to unambiguously resolve this question additional experiments are needed and a combination of grazing incidence small angle X-ray scattering (GISAXS), which is a non-destructive, powerful method to determine cluster shapes, and STM is advisable.

To complete our analysis of the cluster shape, Fig. 3 shows the calculated height–diameter relation for spherical clusters and the measured height–diameter relation of Au-clusters on the C_{60} surface. The calculated values assume a spherical Au-cluster, and the ordinate reflects the diameter, which would be measured by STM for such a cluster. All data from the cluster size distributions shown in Fig. 2 are included in the graph, and the measured heights of the experimentally observed Au-clusters are considerably smaller than those of the hypothetical spherical clusters for all cluster sizes. The cluster shape resembles a half-football or truncated sphere, and is independent of the cluster size with a diameter to height ratio of about 2.5.

In addition to the features described in the previous paragraphs, we observed a reduction of the surface roughness of the fullerene surfaces, which is exposed in between the nanometer sized Au-clusters. The surface features on a molecular scale were quantified by determining the height distributions of fullerene surfaces for two sets of samples:
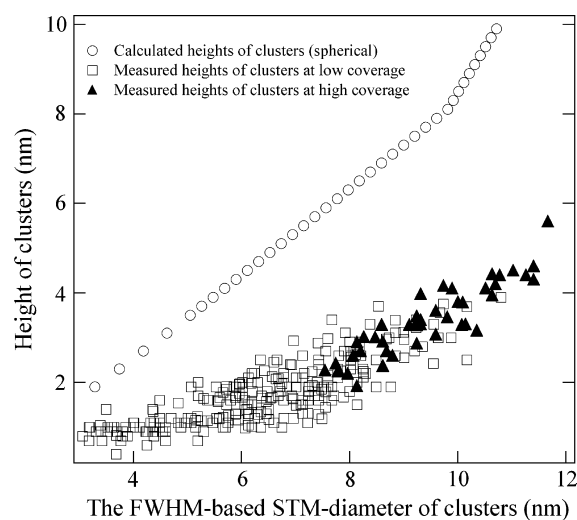

Fig. 3. The graph includes the calculated heights of Au clusters, which are obtained by placing an ideal spherical Au-cluster on a C_{60} surface. The FWHM-diameter (abscissa) is the diameter that these ideal clusters would show in an STM measurement. The experimental data for the measured heights of Au-clusters for the low and high-coverage of Au (Fig. 1b–d) are shown.

pure C_{60}, and low Au-coverage. The exposed fullerene surface areas on the high-coverage sample were too small for a comprehensive analysis, albeit line scans indicate that the same height distribution is present as in the low-coverage samples. Fig. 4 includes a representative graph of all measured heights within the selected image section of the C_{60} surface. The image sections used for analysis contained no Au-clusters, and the image background was corrected to remove the influence of the tilt of the sample surface. In all image sections, the C_{60} molecules were clearly resolved, and several sections were analyzed from each sample, and measurements performed with different tips are included. First and second layer fullerene surface sections yielded identical results. The program WSxM version 4.0 [25] was used to perform this analysis and representative example of the height histograms are shown in Fig. 4. The width of the histograms reflects the difference between the maximum and minimum heights recorded in each image. Only the differences in height are relevant, the absolute height is arbitrary and changes with the overall topography of the whole image frame, and the center of the height histogram is positioned at the origin. A smaller width of the height histogram is associated with a smaller roughness; a larger width corresponds to a rougher sample with larger local height variations. Typical values for the full width at half maximum (FWHM) for fullerene surfaces prior to Au-deposition are between 0.13 and 0.25 nm (datasets from different samples analyzed with different tips). From purely geometric considerations an atomically sharp, long tip with a diameter of 0.2 nm can at most measure a height difference of 0.3 nm between the fullerene top and the depth of the trough between molecules, the diameter of C_{60} is taken as 1 nm. After the deposition of Au, the FWHM of the height distribution is reduced to 0.04–0.09 nm, the depth of the troughs between the molecules is greatly reduced. The reduction in surface roughness is observed for all fullerene surfaces, which were exposed to the Au-atom beam and is independent of the distance to
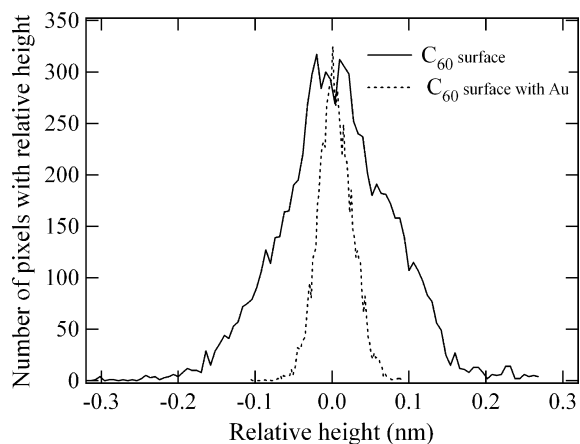
large Au-clusters and the local Au-cluster density (see Fig. 4).

However, STM is sensitive to the topographical as well as electronic changes in the surface, and the presence of Au is known to lead to a band bending and modification of the position of the Fermi energy within the gap of the fullerene solid. The position of the Fermi energy and highest occupied molecular orbital (HOMO) of C_{60} are sensitive to Au-coverage [17], and are expressed in the photoelectron spectroscopy as a rigid shift of all spectral features.

A comparison of the density of states (DOS) for the pure and the Au-covered surface shows an increase in the DOS at 1.2 V, the bias voltage used in our experiments, albeit the STM gap voltage is still located between the highest occupied molecular orbital (HOMO) and the Fermi energy. Keeping all other experimental conditions constant an increase in the DOS would lead to a larger tunneling current and therefore a larger apparent height (and presumable larger surface roughness). However, the spatial distribution of the charge is not reflected in the photoemission data. And this aspect will require an in-depth analysis in the future. Moreover, the surface roughness and apparent height of the fullerene molecules is independent of the concentration or distance to Au-clusters, which supports the interpretation of the surface roughness as a topographic rather than an electronic effect due to charge transfer from the Au-clusters to the C_{60}. We therefore tentatively attribute the spatially homogeneous reduction in surface roughness to a change in topography rather than a modification of the surface electronic structure or redistribution of the surface charge density. We suggest that the troughs in between the fullerene molecules are filled with Au-atoms, which are placed at bonding sites in between the C_{60} spheres. The mobile Au-atoms trapped in the troughs between the fullerene molecules coexist with the larger, nanometer-sized, stationary Au-clusters. The failure to resolve the Au-atoms can be due to the high mobility of individual Au-atoms or the unfavorable geometry of atoms trapped relatively far away from the terminating surface. Deposition experiments at very low Au-coverage and low temperatures might serve in the future to answer this question.

To explore the effects of Au on the growth of fullerene layers, we deposited Au and C_{60} molecules simultaneously on an HOPG surface. In the co-deposition both constituents are highly mobile on the surface. An STM image of the resultant layer is shown in Fig. 5a and a higher resolution image is included in Fig. 5b. The first layer of C_{60} adopts the same characteristic shape of round, elongated islands, which were already observed in the deposition of C_{60} on graphite [19]. The second layer, however, does not form fractal islands, but self-organizes into islands surrounding Au-clusters. Only very few Au-clusters lack the surrounding fullerene ring-structure. The Au-beads at the fullerene island edges, which are characteristic of the Au-deposition on fullerene layers, are missing, and a Au-depletion region along the edges of the first layer C_{60} is observed. Fig. 5b shows a section of the second layer fullerenes and

Fig. 4. Histograms of height distributions which characterize the surface roughness of C_{60} surfaces with and without Au.
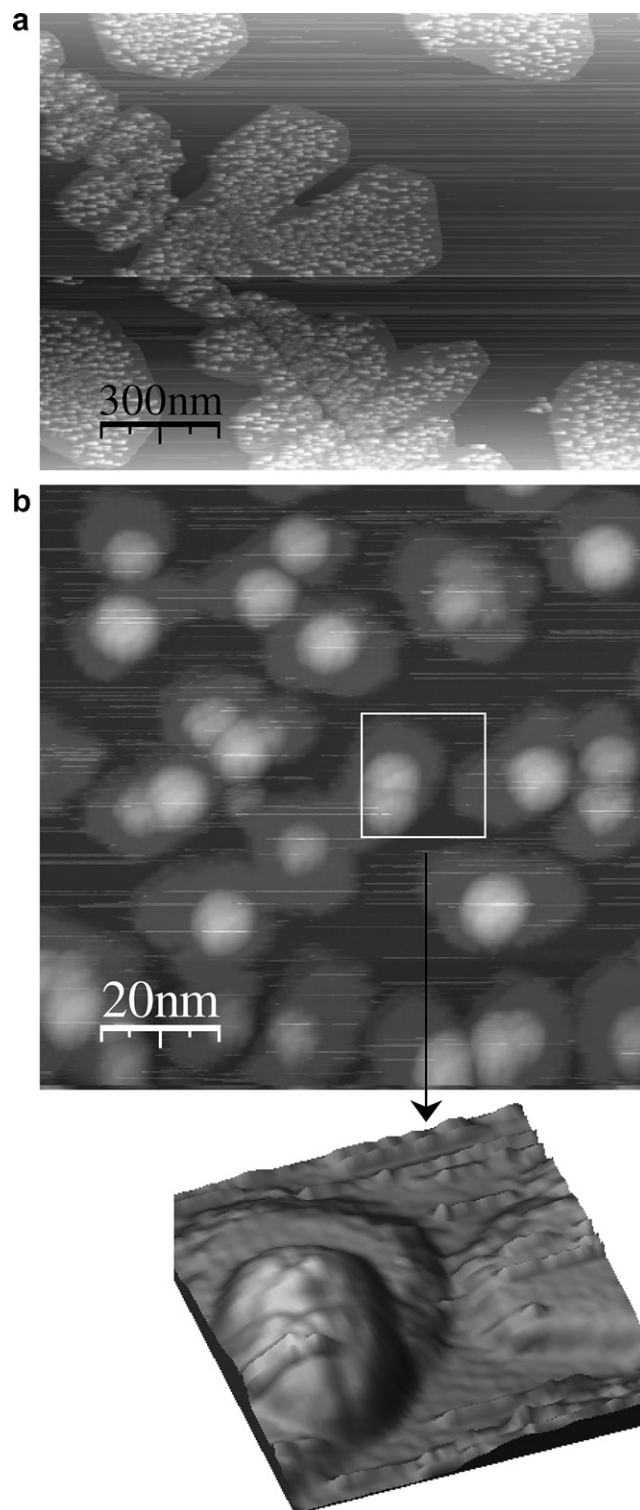
a

300nm

b

20nm

Fig. 5. This figure illustrates the characteristic features of the structure formed during the co-deposition Au and C_{60} on HOPG. (a) Overview of the structures and (b) STM image with high-resolution and 3D depiction of the structure. The individual C_{60} molecules are resolved, which is apparent in the 3D image.
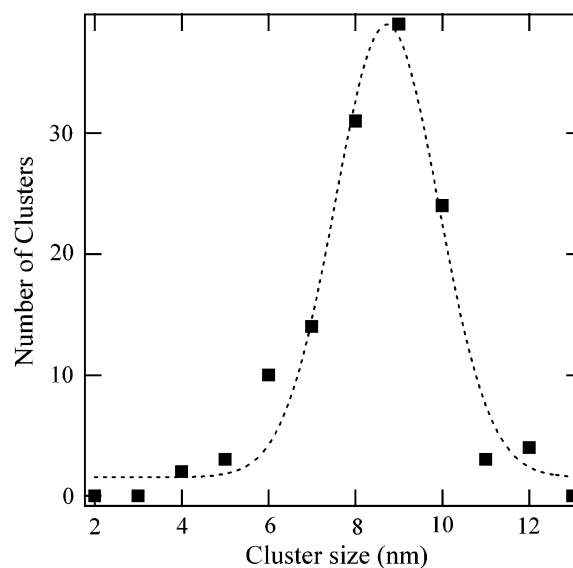

Fig. 6. Lateral size distribution of Au-clusters in the co-deposition system (obtained from images shown in Fig. 5).

size is 8.8 ± 1.3 nm, slightly larger than for the low Au-coverage shown in Fig. 2. The FWHM of the distribution is only about 2 nm, and thus significantly smaller than in the Au-deposition on fullerene surfaces. The width of the fullerene-ring is on average 4 nm, which corresponds to four molecules. If the fullerene flux is reduced, the width of the "fullerene ring" is reduced, and the Au-cluster formation is largely unaffected (images not shown here).

4. Discussion

The most striking observations in the positioning of the Au-clusters on the fullerene surface are the accumulation of clusters on the graphite–fullerene edge, the increased density of Au-clusters on the second layer fullerene islands and the lack of preferential nucleation at the fullerene–fullerene steps. The formation of critical nuclei is the first step in a cluster growth process, and can be promoted by the presence of nucleation centers such as edges and kinks, which are often preferred bonding sites. The graphite–fullerene edge clearly serves in this role, while no preferential condensation occurs on the fullerene–fullerene step. The subsequent nucleation and growth of clusters requires a flux of atoms, which supersedes the loss/evaporation of atoms from the cluster surface. If the incoming atom flux is insufficient to provide the requisite supersaturation the cluster will dissolve and the probability of forming a stable nucleus is greatly diminished. The positioning of the clusters right on the graphite–fullerene edge indicates that the Au-atom supply for the edge clusters is provided by diffusion across the fullerene as well as the graphite surface. It is also observed, see Fig. 1c, that areas of the edge which are adjacent to only small sections of exposed graphite surface, exhibit a smaller number of edge clusters while the cluster "beads" are completely closed for higher

fullerene rings around the Au-clusters, the dark regions between the clusters are the first layer fullerenes. The cluster size distribution is shown in Fig. 6, and the average cluster

Au-coverage. In contrast to the graphite–fullerene edge, the fullerene–fullerene edge does not act as a nucleation center. The lack of edge decoration can be caused by a comparatively lower adatom mobility on the fullerene surface, which will favor nucleation on terraces rather than at step edges, or a relatively small binding energy of Au atoms at the fullerene–fullerene edge, which will favor detachment from the step. A comparatively higher Au-adatom mobility and/or edge attachment energy on the graphite surface [22] is commensurate with the observed preferential nucleation at the graphite–C_{60} edge.

Although the initial density of Au-atoms is equal on all areas of the surface, the first C_{60} layer shows a considerably lower density of Au-clusters than the second layer, which is densely populated with Au-clusters and retains its original shape. If we assume that the Ehrlich–Schwoebel barrier prevents most clusters and atoms from crossing the C_{60}–C_{60} step edge, the depletion of the Au-supply due to the formation of the Au-clusters at the graphite–C_{60} edge will consequently lead to the cluster depletion on the first layer fullerene layer. Interestingly there are no significant differences in the cluster size distribution between the first and second C_{60} layers, which indicates a similar growth rate on both surfaces and a selective suppression of nucleation on the first layer.

It is somewhat surprising that the specific fractal structure of the second layer C_{60} islands is preserved quite well even for the high Au coverage. Previous studies on the interaction of C_{60} with Au surfaces and vice versa indicated a strong interaction, charge transfer and chemisorption of C_{60} on Au [12,17,21,26] and C_{60} molecules can even trigger the reorganization of Au-surface and initiate the movement of Au-edge and kink atoms [8,20]. However, moving fullerene molecules out of the fullerene islands to maximize the contact area with the nanometer sized Au-clusters is apparently not energetically favorable, and the fullerene structures remains unchanged.

Although the nanometer-sized Au-clusters are the most prominent feature in the STM images, the roughness analysis strongly indicates the presence of an inventory of highly mobile Au-atoms or ultrasmall Au-cluster, which are positioned in the troughs between the C_{60} molecules and coexist with the larger Au-clusters. The high-coordination number sites in the troughs provide energetically favorable bonding positions, and the cluster growth likely commences once these relatively few favorable sites are filled.

The growth mechanism during the co-deposition of Au and C_{60} on graphite is clearly different from that of the sequential deposition discussed in the previous section, and leads to the formation of striking self-organized cluster assemblies. While in the sequential deposition of C_{60} on Au or vice versa, only one of the reactants is highly mobile and the other one already bound in a solid, during the co-deposition experiment both reactants are highly mobile on a weakly interacting substrate surface. The structure assembly is driven by the competition between the Au- and fullerene interaction and self-interaction: the high cohesive energy of Au favors the formation of Au-clusters, the chemisorptive interaction between fullerenes and Au leads to the formation of the fullerene ring around the individual Au-clusters. A passivation of the Au-clusters by the surrounding C_{60} molecules could lead to a self-limiting growth process similar to the one reported by Wang [15] in the Ag–C_{60} system, which controls the size of Au-clusters and thus leads to the relatively narrow size distribution (see Fig. 6).

5. Conclusions

In summary, we observed the deposition of Au on C_{60} layers, which were grown on HOPG at room temperature, and performed a detailed analysis of the spatial distribution of Au and Au-clusters, their size distribution and shape. An analysis of the effect of tip-convolution on the size distribution and shape is included. The Au-clusters are concentrated on the C_{60} terminated surface section, which preserves its characteristic fractal-dendritic features, and preferentially nucleate at the C_{60}–graphite edges, while the C_{60}–C_{60} step edges remain undecorated. In addition, the Au-clusters on C_{60} are immobile, which is in contrast to the high mobility of Au-clusters on graphite surfaces, and are thus suitable for future analysis of the electronic characteristics of ultrasmall Au-clusters with local probes such as STM. The spatial distribution of the clusters can be linked to the specific properties of surface bonding sites, and adatom mobilities on graphite and C_{60}. The nanometer sized Au-clusters coexist with a mobile Au-inventory, which is comprised of Au-atoms or very small clusters positioned in the depressions and troughs in between the C_{60} molecules. This Au-network, which is defined by the surface corrugation of the fullerene surface, might provide conducting pathways on the surface independent of the percolation pathways formed by nanometer-sized clusters. A rather small amount of Au could therefore be sufficient to provide electrical contact to the fullerene layer and might open a new strategy for electrical contacting of photoactive regions in the design of multilayer organic solar cells.

Finally, the self-organization of fullerenes in islands surrounding the Au-clusters was observed when Au and C_{60} were co-deposited on HOPG; a structure which will be explored in more detail in the future. Future experiments will focus on the investigation of the initial stage of deposition of other metal elements on C_{60} layers, and the formation of self-organized metal–fullerene structures.

References

[1] L. Forro, L. Mihaly, Rep. Prog. Phys. 64 (2001) 649.
[2] R.C. Haddon, A.S. Perel, R.C. Morris, T.T.M. Palstra, A.F. Hebard, R.M. Fleming, Appl. Phys. Lett. 67 (1995) 121.
[3] A.P.G. Robinson, R. Palmer, T. Tada, T. Kanayama, J.A. Preece, Appl. Phys. Lett. 72 (1998) 1302.
[4] H. Shinohara, Rep. Prog. Phys. 63 (2000) 843.
[5] Y.P. Sun, J.E. Riggs, Int. Rev. Phys. Chem. 18 (1999) 43.
[6] C. Chavy, C. Joachim, A. Altibelli, Chem. Phys. Lett. 214 (1993) 569.
[7] S. Licht, O. Khaselev, P.A. Ramakrishnan, D. Faiman, E.A. Katz, A. Shames, S. Goren, Solar Energy Mater. Solar Cells 51 (1998) 9.
[8] J.K. Gimzewski, C. Joachim, Science 283 (1999) 1683.
[9] J.K. Gimzewski, S. Modesti, R.R. Schlittler, Phys. Rev. Lett. 72 (1994) 1036.
[10] S. Guo, D.P. Fogarty, P.M. Nagel, S.A. Kandel, J. Phys. Chem. B 108 (2004) 14074.
[11] A. Marchenko, J. Cousty, Surf. Sci. 513 (2002) 233.
[12] T.R. Ohno, Y. Chen, S.E. Harvey, G.H. Kroll, P.J. Benning, J.H. Weaver, L.P.F. Chibante, R.E. Smalley, Phys. Rev. B 47 (1993) 2389.
[13] Z.Y. Rong, L. Rokhinson, Phys. Rev. B 49 (1994) 7749.
[14] L. Ruan, D.M. Chen, Surf. Sci. 393 (1997) L133.
[15] H. Wang, J.G. Hou, O. Takeuchi, Y. Fujisuku, A. Kawazu, Phys. Rev. B 61 (2000) 2199.
[16] A.F. Hebard, C.B. Eom, Y. Iwasa, K.B. Lyons, G.A. Thomas, D.H. Rapkine, R.M. Fleming, R.C. Haddon, J.M. Philips, J.H. Marshall, R.H. Eick, Phys. Rev. B 23 (1994) 17740.
[17] H. Kroeger, P. Reinke, J. Chem. Phys. 123 (2005) 114706.
[18] P. Reinke, P. Oelhafen, Phys. Rev. B 71 (2005) 045420.
[19] H. Liu, P. Reinke, J. Chem. Phys. 124 (2006) 164707.
[20] L. Bartels, G. Meyer, K.H. Rieder, Phys. Rev. Lett. 79 (1997) 697.
[21] O. Kurnosikov, J.T. Kohlhepp, W.J.M.D. Jonge, Surf. Sci. 566–568 (2004) 175.
[22] H. Hoevel, I. Barke, Prog. Surf. Sci. 81 (2006) 53.
[23] D. Klyachko, D.M. Chen, Surf. Sci. 446 (2000) 98.
[24] Y. Hasegawa, I.W. Lyo, P. Avouris, Appl. Surf. Sci. 76–77 (1994) 347.
[25] I. Horcas, R. Fernandez, J.M. Gomez-Rodriguez, J. Colchero, J. Gomez-Herrero, A.M. Baro, Rev. Sci. Instr. 78 (2007) 013705.
[26] M. Pedio, R. Felici, X. Torrelles, P. Rudolf, M. Capozi, F. Rius, S. Ferrer, Phys. Rev. Lett. 85 (2000) 1040.
[27] C. Petit, T. Cren, D. Roditchev, W. Sacks, J. Klein, M.-P. Pileni, Adv. Mater. 11 (1999) 1198.
[28] F. Silly, A.O. Gusev, A. Taleb, F. Charra, M.-P. Pileni, Phys. Rev. Lett. 84 (2000) 5840.
[29] K. Majumdar, S. Hershfield, Phys. Rev. B 57 (1998) 11521.